Asian Journal of Chemistry; Vol. 35, No. 5 (2023), 1113-1122

ASIAN JOURNAL OF CHEMISTRY

https://doi.org/10.14233/ajchem.2023.27624

Multivariate Statistical Analysis of Spatial and Vertical Distribution of Radiological, Mineralogical and Magnetic Parameters of Beach Sediments from North East Coast of Tamilnadu State, India

S. SENTHIL[1], V. RAMASAMY[2], K. PARAMASIVAM[3] and G. SURESH[4,*]

[1]Department of Physics, Panimalar Engineering College, Poonamallee, Chennai-600123, India
[2]Department of Physics, Annamalai University, Annamalai Nagar-608002, India
[3]Department of Physics, MRK Institute of Technology, Kattumannarkoil-608301, India
[4]Department of Physics, Aarupadai Veedu Institute of Technology, Vinayaka Mission's Research Foundation, Chennai-603104, India

*Corresponding author: E-mail: senthilram1982@gmail.com

Received: 10 February 2023; *Accepted*: 3 April 2023; *Published online*: 28 April 2023; AJC-21218

The γ-ray spectroscopic technique has been effectively utilized to know the activity concentrations of ^{238}U, ^{232}Th and ^{40}K in different depths of north-east coast beaches of Tamilnadu state of India. The measured activity concentrations were different while compare from surface to second feet depth. FTIR exhibits the presence of eleven minerals such as quartz, feldspar in different phases, kaolinite, gibbsite, calcite, organic carbon, aragonite, palygorskite and hematite in all feet sediments. Extinction coefficient calculation shows that the amount major minerals is in the order of kaolinite < microcline feldspar < quartz. Different minerals were identified through XRD analysis. Multivariate statistical was also adopted well and the results confirm that the magnetic susceptibility play a major role in controlling the present radioactivity values. The activity concentration of ^{238}U, ^{232}Th and ^{40}K for >125 µm grain sized samples are significantly lowered when compared with the respective values of the bulk samples.

Keywords: Radioactivity, Minerals, Magnetic susceptibility, Multivariate statistical analysis, Beach sediment.

INTRODUCTION

Availability of natural radionuclides (^{238}U, ^{232}Th and ^{40}K) and their health effects to the human beings (acute leucopenia, anemia, leukemia, necrosis of the mouth, tooth fracture, pancreatic liver, hepatic, bone and kidney cancers) in various geological settings include rocks, beaches, sediments, minerals and building materials due to the local geology, geochemical behaviour and anthropogenic activities are unavoidable [1-3]. Interestingly, aforementioned presence and health effects could be related to the natural radioactivity which occupies 85% to the total global annual average ionizing radiation [4]. To assess the complete radiological risks and relevant dependence parameters of the important topographical place of communication between earthly and aquatic networks called beaches, study of natural radioactivity in concern sediments is essentially to be executed [5].

Now a day's many manmade activities and geological setting disturbance at around coastal areas especially beaches could be possible. It is well-known that 40% of the world's population lives within 100 km of the coast. A wide majority of countries have a large percentage of their population (80-100%) living within the 100 km boundary [6] and also settlements are being concentrated within 5 km of the coastline [7]. These remarkable establishments could be available along the north-east coast of Tamilnadu state, India and were reported earlier [8]. Therefore, the determination of natural radionuclides in beaches of north-east coast of Tamilnadu is essential, which was carried out for the upper surface sediments and reported in the previous articles [9-11]. To know the complete radiological characterization of above said beaches, the present study has planned to study the radioactivity and relevant parameters in further depth (first and second feet) sediments. To achieve the goal, radioactivity data of upper surface sediment were taken for comparison [9-11].

Coastal beaches are mostly made up of sediments and sands that have been weathered and transported by water or glaciers and force of gravity [1]. Most of the coastal beach sands

or sediments contain various minerals such as quartz, feldspar, monazite, zircon and other magnetic minerals, some of them potentially contribute to the marine radioactivity [1,12]. During the mineral formations, the radionuclides could be incorporated as trace elements in their crystal lattice of minerals such as heavy, trace, magnetic and clay minerals [13]. Many studies suggest that the mineral and magnetic parameters have been recognized as simple and alternative tool for determining radioactivity level in river, marine, estuarine and fluvial sediments [14,15]. Hence, the accumulation and distribution of radionuclides depend mostly on grain size, mineral and magnetic parameters of the sediments.

The main objective of this study is to (i) determine the activity concentrations (Bq/kg) of ^{238}U, ^{232}Th, ^{40}K and calculate the absorbed dose rate (D) (nGy/h) in different depth (upper surface, first and second feet) beach sediments of north east coast of Tamil nadu state of India; (ii) identify the minerals through FTIR, XRD and measure the magnetic susceptibility in all depth sediments; (iii) find the interrelationship between radiological [^{238}U, ^{232}Th, ^{40}K and absorbed dose rate (D)], mineralogical and magnetic parameters of the beach sediment using the multivariate statistical analysis and finally, (iv) measure the activity concentrations (Bq/kg) of ^{238}U, ^{232}Th and ^{40}K in after removal of lower grain sized samples (< 125 mm) from upper surface.

EXPERIMENTAL

Study area: The study area begins from Parangipettai (Porto-novo), which is close to the Vellar river estuary and ends in Marina beach, Chennai city which is near to Coouam river estuary (lies between 11º30′0.935 N and 13º03′0.974 N latitude and 79º46′0.279 E and 80º17′0.362 E longitude). It covers more than 200 km and includes four coastal districts (Chennai, Kanchipuram, Villupuram and Cuddalore) and union territory of Pudhucherry. Other important details of the study area were clearly given in our earlier work [8].

Sample collection: From the total length (approximately 200 km), 35 places were successively chosen (S_1 to S_{35}) with distance interval of 5 to 6 km (Fig. 1). Three samples (upper surface, first and second feet) were collected manually at each sampling location during a dry period using a plastic spade (roughly 3 kg) and then stored in polyethylene bags.

Sample preparation and instruments used: The γ-ray spectrometer with NaI (Tl) crystal detector of size 3″ × 3″ along with 8K multichannel analyzer was used to record the γ-ray spectra. The below detectable limits (BDL) of ^{238}U and ^{232}Th radionuclide were 5.5 Bq/kg and 21.5 Bq/kg for ^{40}K, which could be determined from the background radiation spectrum for the same counting time as for sediment samples. Minerals characterizations were carried out by using the Perkin-Elmer RX1 FTIR spectrometer and Seifert (JSO-DEBYEFLEX 2002) X-ray diffractometer magnetic susceptibility measurements were carried out using a magnetic susceptibility meter, Bartington Instruments Ltd., linked to MS2B dual frequency sensor (0.47 and 4.7 KHz). Sample preparation, procedure and other technical details of instruments are already reported in our earlier works [8-10,13].

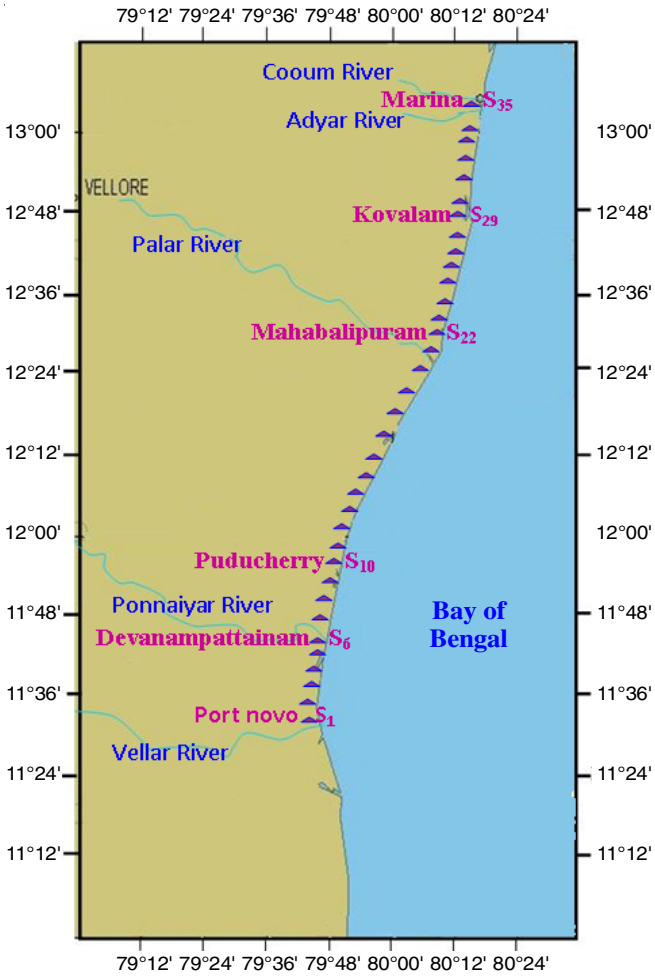

Fig. 1. Geographic location of North East coast of Tamilnadu where the sediment samples were collected

RESULTS AND DISCUSSION

Radioactivity analysis: Horizontal and vertical (upper, first and second feet samples) distribution of radionuclides

Table-1 presents the activity concentrations (Bq/kg) of ^{238}U, ^{232}Th and ^{40}K in different depth (upper, first and second feet) beach sediment samples and their distributions are shown in Fig. 2. The measured activity concentrations range from BDL to 30.42 ± 7.90 Bq kg^{-1} for ^{238}U, BDL to 218.64 ± 8.02 Bq kg^{-1} for ^{232}Th and 212.6 ± 24.68 to 423.43 ± 26.52 Bq kg^{-1} for ^{40}K in upper surface samples, BDL to 14.44 ± 8.55 Bq kg^{-1} for ^{238}U, BDL to 290.94 ± 9.55 Bq kg^{-1} for ^{232}Th and 211.03 ± 27.97 to 392.87 ± 36.12 Bq kg^{-1} for ^{40}K in first feet samples, BDL to 11.60 ± 6.13 Bq kg^{-1} for ^{238}U, BDL to 77.75 ± 5.89 Bq kg^{-1} for ^{232}Th and 206.19 ± 23.75 to 404.22 ± 27.42 Bq kg^{-1} for ^{40}K in second feet samples.

Due to mineralogy and drainage pattern of the study area, radionuclides activities are widely varied in various sites of upper, first and second feet sediments [9,10]. Activity concentration trends are not uniform from surface to deeper depth since the depositions of radioactivity minerals in the past was not uniform. However, it is very clear that the mean activity concentration of ^{238}U is decreased and ^{40}K is increased towards the deep. A random variation of ^{232}Th is observed while sea

TABLE-1
BASIC STATISTICAL DATA FOR ACTIVITY CONCENTRATIONS OF ^{238}U, ^{232}Th, ^{40}K AND ABSORBRD DOSE RATE (D) IN DIFFERENT DEPTH SEDIMENTS

	Activity concentration of radionuclides (Bq/kg)			Absorbrd dose rate (D) (nGy/h)
	^{238}U	^{232}Th	^{40}K	
Upper surface				
Mean	8.31 ± 4.88	24.52 ± 4.73	275.97 ± 25.58	30.17 ± 6.11
Maximum	30.42 ± 7.90	218.64 ± 8.02	423.43 ± 26.52	156.73 ± 9.58
Minimum	BDL	BDL	212.60 ± 24.68	15.63 ± 3.50
Std. Dev	5.42	47.01	63.66	30.76
CV (%)	65.21	191.75	23.07	101.95
Skewness	3.42	3.53	0.93	3.44
Kurtosis	11.51	11.94	-0.39	11.58
First feet				
Mean	7.80 ± 4.55	38.20 ± 5.01	298.15 ± 26.57	39.11 ± 6.24
Maximum	14.44 ± 8.55	290.94 ± 9.55	392.87 ± 36.12	197.46 ± 11.41
Minimum	BDL	BDL	211.03 ± 27.97	16.16 ± 3.36
Std. Dev	2.06	53.39	51.58	33.85
CV (%)	26.47	139.75	17.30	86.54
Skewness	1.32	3.57	-0.01	3.44
Kurtosis	1.89	15.11	-1.26	14.31
Second feet				
Mean	6.64 ± 3.14	11.58 ± 3.89	299.37 ± 25.73	22.55 ± 4.88
Maximum	11.60 ± 6.13	77.75 ± 5.89	404.22 ± 27.42	64.70 ± 7.48
Minimum	BDL	BDL	206.19 ± 23.75	14.53 ± 3.37
Std. Dev	1.45	12.48	51.31	8.79
CV (%)	21.79	107.74	17.14	38.98
Skewness	1.83	4.68	0.08	3.50
Kurtosis	3.17	24.58	-0.81	15.61
Recommended level (UNSCEAR, 2000)	33	45	420	57

Note: Std. Dev: Standard deviation; CV: Coefficient of variability (%)

from upper to second feet depth. It is obvious from Table-1 that the high mean activity concentration of ^{238}U, ^{232}Th and ^{40}K are observed in upper surface, first and second feet samples. Uosif *et al.* [16] observed the higher concentrations of ^{40}K in deeper depths of Safaga beach, Egypt. Sutherland & de Jong [17] observed the same decreasing trend of ^{238}U towards the depth in different locations of Canada coast at the intervals of 0-15 cm and 15-30 cm, which may be due to the leachable nature of ^{238}U. The ^{40}K activity could be controlled by resistant organic matter, ordered crystalline oxide material and clay lattices [18].

In upper surface and first feet of Mahabalipuram beach (S_{22}), due to the presence of black sands enriched with mineral monazite, activity concentration of ^{238}U (30.42 ± 7.90 Bq kg^{-1}) and ^{232}Th (290.94 ± 9.55 Bq kg^{-1}) are high [16]. Likewise, as reported earlier [9-11], when compared with studied depths, in upper surface of Kovalam beach (S_{29}), activity concentration of ^{40}K (423.43 ± 26.52 Bq kg^{-1}) is high which is controlled by major minerals such as feldspar and micas [19] and higher amount of clay minerals [20].

The lowest activity concentration of ^{238}U (BDL) was found in 4 sites (S_{10}, S_{27}, S_{33} and S_{35}) of upper surface samples, 4 sites (S_3, S_8, S_{10} and S_{13}) of first feet samples and 9 sites (S_3, S_4, S_7, S_9, S_{10}, S_{13}, S_{16}, S_{17} and S_{33}) of second feet samples. Low concentration of ^{232}Th (BDL) was found in the upper surface of Pudhuchery beach (S_{10}), 2 sites (S_3 and S_{10}) of first feet samples and 4 sites (S_8-S_{10} and S_{16}) of second feet samples. The lowest activity concentration of ^{40}K (206.19 ± 23.75 Bq kg^{-1}) is found at S_{17} of upper surface. According to Jankovic *et al.* [21], the lowest activity concentrations of the radionuclides in sediments may be linked with less contribution of human activity and presence of high content of quartz.

To know the radiological hazard status basically, studied activity concentrations need to be compared with world average data (Table-1). The world averages of ^{238}U, ^{232}Th and ^{40}K in sediments were 33, 45 and 420 Bq kg^{-1} respectively [4]. From Table-1, it is confirmed that the mean activity concentrations of ^{238}U, ^{232}Th and ^{40}K in all studied depths are within the world average values. When observe the site wise, ^{38}U concentrations of all sites of all depths are lower than world average value (represented in yellow colour horizontal line) (Fig. 2). In case of ^{232}Th, three sites of upper surface, eight sites of first feet and one site from second feet exhibit the higher values than corresponding world average values. Only two sites of upper surface show the high values (^{40}K).

Univariate statistical analysis (distribution of radionuclides): The measured activity concentrations (^{238}U, ^{232}Th and ^{40}K) of samples from all studied depths have been applied into Univariate statistical analysis (Table-1) and the histograms of activity concentrations are shown in Fig. 3. The ^{238}U and ^{40}K exhibit high degree of uniformity, while ^{232}Th displays the low degree of uniformity in all studied depths. Concentrations of ^{238}U and ^{40}K radionuclides show low degree of mobility since the co-efficient of variance (CV %) values are below 100%, whereas concentration of ^{232}Th shows high degree of mobility

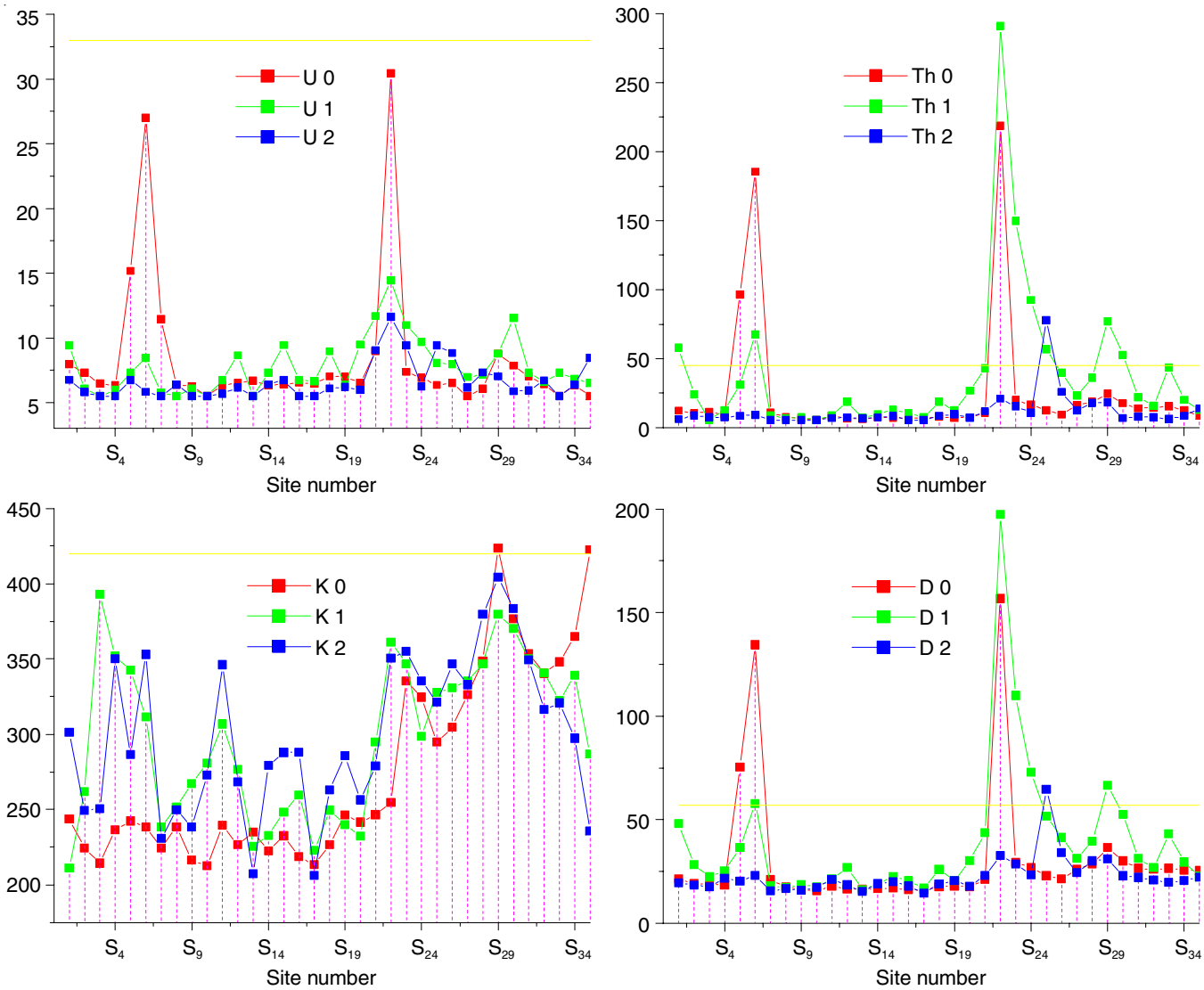

Fig. 2. Activity concentrations (Bq/kg) of ^{238}U, ^{232}Th and ^{40}K radionuclides in different depth beach sediment samples

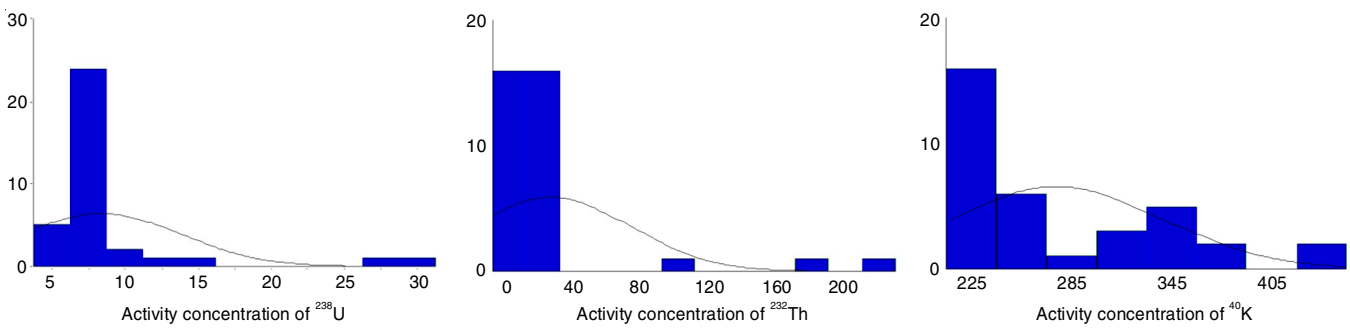

Fig. 3. Frequency distribution of ^{238}U, ^{232}Th and ^{40}K (upper surface samples)

since the coefficient of variance (CV %) values are above 100% [22,23] in all studied depths.

All the studied activity concentrations (except first feet of ^{40}K) in all feet exhibit asymmetric distributions. Their values plotted on graph do not give bell shaped form (Fig. 3; derived for upper surface) and its positive values indicate the positive skewness. Kurtosis is a measure of peakedness. Depends upon the peakedness, it is named as mesorkurtic (kurtosis = zero), leptokurtic (kurtosis = positive) and platy kurtic (kurtosis = negative). In the present study, the kurtosis values of activity concentrations of ^{238}U and ^{232}Th are positive, which indicates the curve is more peaked than the normal curve (*i.e.*) lepto-kurtic. Negative kurtosis values are observed for ^{40}K concentration which indicates platy kurtic (less peaked). This is due to the uneven spatial distribution of radionuclides in the sediments of north east coast of Tamilnadu [22,23].

Absorbed dose rate calculation (D): To evaluate the health risk of the present beach sediments, the total absorbed dose rate (D) (nGy/h) is calculated using the following formula [24]:

$$D = (0.462\ C_U + 0.604\ C_{Th} + 0.0417\ C_K)\ nGy/h$$

where C_U, C_{Th} and C_K are the activity concentrations (Bq/kg) of ^{238}U, ^{232}Th and ^{40}K in beach sediments, respectively. Table-1 presents the calculated values of absorbed dose rate in all foot and its spatial distribution are visualized in Fig. 2. It is ranged from 15.63 nGy h^{-1} to 156.73 nGy h^{-1} with an average value of 30.17 nGy h^{-1} for upper surface samples, 16.16 nGy h^{-1} to 197.46 nGy h^{-1} with an average value of 39.11 nGy h^{-1} for first feet samples and 14.53 nGy h^{-1} to 64.70 nGy h^{-1} with an average value of 22.55 nGyh^{-1} for second feet samples. The mean absorbed dose rates of all depth samples are within the world average values (57 nGy h^{-1}) [4]. Three sites of upper surface and five sites of first feet samples show high absorbed dose values when compared with world average value.

Horizontal and vertical (upper, first and second feet samples) distribution of minerals

FTIR studies: The FTIR spectra were recorded for all the samples of different depth beach sediments. A representative FTIR spectrum of second feet sample of S_{22} is shown in Fig. 4. The observed wave numbers are analyzed and the minerals are assigned (Table-2) using available literatures [9,24-35]. The minerals such as quartz, feldspar (microcline, orthoclase and albite), kaolinite, gibbsite, calcite and organic carbon are identified in upper surface samples. Almost all the minerals present in upper surface are same as in first and second feet samples with slight variations in the intensities of the peaks. Three additional minerals (palygorskite, aragonite and hematite) were also observed in first and second feet samples.

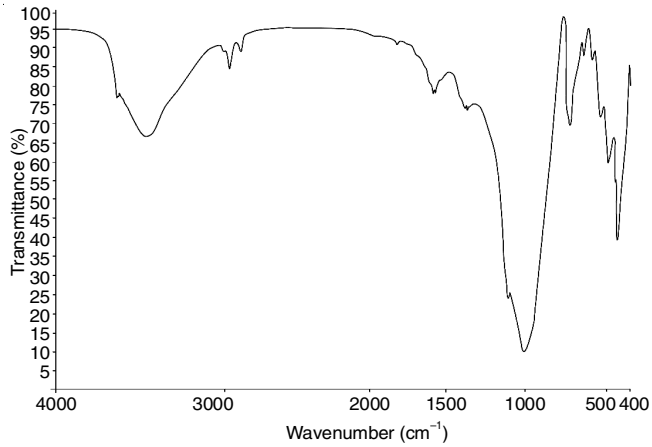

Fig. 4. FTIR spectrum of 2nd feet sample of site number 22

The presence of quartz in the samples can be ascribed by the observation of the peaks in the ranges 462-458 and 514-510 cm^{-1} due to Si-O asymmetrical bending vibrations, 694-690 cm^{-1} due to Si-O symmetrical bending vibrations and 780-776 and 800-796 cm^{-1} due to Si-O symmetrical stretching vibrations, while the 1084-1080 and 1164-1160 cm^{-1} absorption region arises from the Si-O symmetrical stretching vibrations due to low Al for Si substitution. Absorption peaks in the ranges 1614-1610 and 1874-1870 cm^{-1} also indicate the presence of quartz weathered from metamorphic origin [25,28].

The peak pertaining in the range 585-581 cm^{-1} (O-Si-(Al)-O bending vibration), 650-646 cm^{-1} (Al-O coordination) and 1012-1008 cm^{-1} in the samples indicates the presence of micro-

TABLE-2
OBSERVED ABSORPTION WAVE NUMBERS AND CORRESPONDING MINERALS FROM FTIR SPECTRA FOR ALL FEET SAMPLES

Name of the minerals	Observed wavenumber (cm^{-1})	Site number		
		Upper surface	First feet	Second feet
Quartz	462-458	S_1-S_{35}	S_1-S_{35}	S_1-S_{35}
	514-510	S_1-S_{35}	S_1-S_{35}	S_1-S_{35}
	694-690	S_1-S_{35}	S_1-S_{35}	S_1-S_{35}
	780-776	S_1-S_{35}	S_1-S_{35}	S_1-S_{35}
	800-796	S_1-S_{35}	S_1-S_{35}	S_1-S_{35}
	1084-1080	S_1-S_{35}	S_1-S_{35}	S_1-S_{35}
	1164-1160	S_1-S_{35}	S_1-S_{35}	S_1-S_{35}
	1614-1610	S_1-S_{35}	S_1-S_{35}	S_1-S_{35}
	1874-1870	S_1-S_{35}	S_1-S_{35}	S_1-S_{35}
Microcline feldspar	585-581	S_1-S_{35}	S_1-S_{35}	S_1-S_{35}
Orthoclase feldspar	650-646	S_1-S_4, S_6-S_{17}, S_{19}-S_{35}	S_2-S_4, S_6-S_{14}, S_{16}, S_{17}, S_{19}-S_{22}, S_{24}-S_{35}	S_2-S_4, S_6-S_{12}, S_{14}, S_{16}, S_{17}, S_{19}, S_{21}, S_{22}, S_{24}-S_{31}, S_{33}-S_{35}
Albite feldspar	1012-1008	S_1, S_{12}, S_{14}-S_{18}, S_{20}-S_{30}, S_{32}-S_{35}	S_1, S_{11}, S_{12}, S_{14}, S_{16}, S_{17}, S_{18}, S_{20}, S_{21}, S_{24}- S_{28}, S_{30}, S_{32}-S_{34}	S_{11}, S_{12}, S_{14}, S_{16}, S_{18}, S_{20}, S_{21}, S_{24}- S_{28}, S_{30}, S_{32}-S_{34}
Kaolinite	3400-3396	S_1-S_{35}	S_1-S_{35}	S_1-S_{35}
	3625-3621	S_1-S_{35}	S_1-S_{35}	S_1-S_{35}
Gibbsite	670-666	S_1-S_{35}	S_1-S_{35}	S_1-S_{35}
Calcite	1425-1421	S_{32}	S_1, S_3, S_6, S_8, S_{10}, S_{11}, S_{13}, S_{15}, S_{23}, S_{35}	S_6, S_8, S_{10}, S_{11}, S_{15}, S_{22}
Organic carbon	2924 & 2854	S_1-S_{35}	S_1-S_{35}	S_1-S_{35}
Aragonite	1459-1455	–	S_1, S_8, S_{23}, S_{29}, S_{32}, S_{35}	S_1, S_8, S_{29}, S_{32}
Palygorskite	1648-1642	–	S_{13}, S_{15}, S_{20}, S_{32}	S_3, S_{15}, S_{17}, S_{22}, S_{32}
	1680-1676	–	S_1, S_3, S_8, S_{15}, S_{17}, S_{20}, S_{32}, S_{35}	S_1, S_3, S_{29}, S_{32}, S_{35}
	3615-3611	–	S_6, S_8, S_{10}, S_{13}, S_{32}, S_{35}	S_6, S_{13}, S_{22}, S_{35}
Hematite	533-532	–	S_{22}, S_{35}	S_{22}

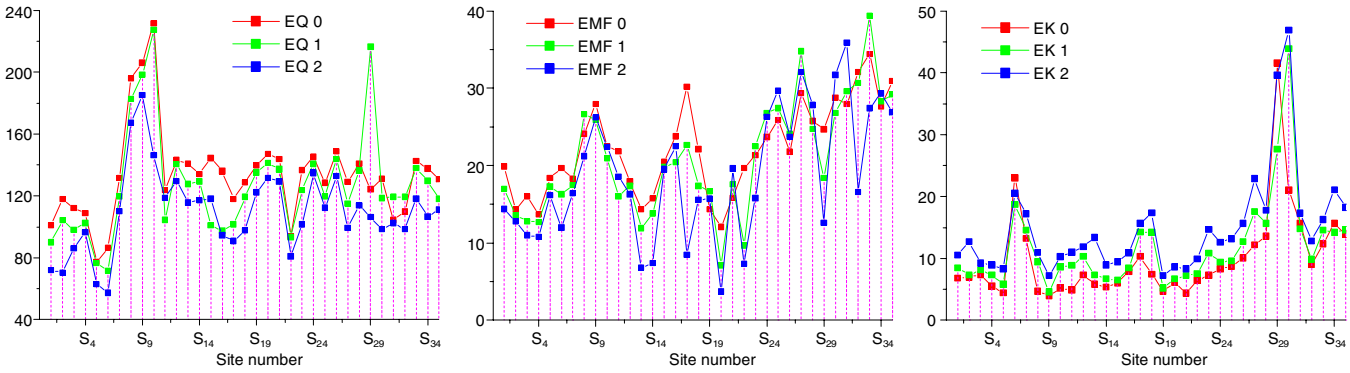

Fig. 5. Extinction co-efficient values of all depth samples

cline feldspar, orthoclase feldspar and albite feldspar ($NaAlSi_3O_8$; Na-feldspar), respectively [30]. The presence of the bands at around 3623 and 3398 cm^{-1} (OH *str.* vibration) are due to the clay mineral kaolinite. As the depth increases from upper to second feet, the intensity of the bands of kaolinite progressively increased and shifted. This suggests that the content of kaolinite increases with disorderedness as depth increases due to leaching [31].

The mid infrared region (1500-1400 cm^{-1}) of the spectra is dominated by the vibrational modes of carbonate ions. According to Adler & Kerr [26], when calcite mineral predominates in an aggregate the peak appears at 1423 cm^{-1}. The trihydrate aluminium mineral gibbsite is identified by the observation of the peak in the range 670-666 cm^{-1}. Appearing peaks at 2854 and 2924 cm^{-1} in all the samples show the presence of organic carbon [30].

In present study, a peak in the range 1648-1642 cm^{-1} and 1680-1676 cm^{-1} were observed only in few sites of first feet and second feet. The presence of OH stretching band at 3615-3611 cm^{-1} in few sites of first and second feet samples represents the presence of palygorskite [30]. The peak observed in the range 1459-1455 cm^{-1} indicates the presence of aragonite mineral [10]. It is distinct from calcite (rhombohedral), which indicates its presence in some sites of first and second feet samples. Hematite is the most abundant iron mineral, which is identified in 2 sites (S_{22} and S_{35}) in first feet and only one site (S_{22}) in second feet samples, which may be due to the replacement of Fe in the samples [29].

Relative distribution of quartz, microcline feldspar and kaolinite: The extinction coefficient values of major minerals (quartz, microcline feldspar and kaolinite) were calculated [24] for all depth samples and the values are presented in Fig. 5. In all depth, it was observed that three minerals are distributed randomly. In overall view, the amount of kaolinite is lesser than feldspar and very much lesser than quartz in all the sites, which are visually indicated in Fig. 5. It is observed that the amount of quartz and feldspar is decreased and kaolinite is increased from upper to deeper depth in almost all the sites. This may be due to leaching of quartz and feldspar [31].

XRD studies: The X-ray diffractograms were recorded for all depth samples and representative diffractogram (second feet sample of S_{22}) is shown in Fig. 6. From the XRD patterns, the minerals identified in upper surface are quartz, orthoclase

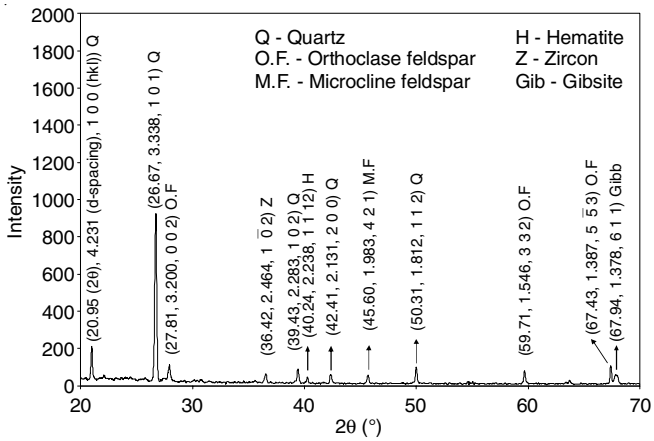

Fig. 6. X-ray diffraction pattern of sample of site number S_{22} of second feet

feldspar, microcline feldspar, albite, zircon, monazite, hematite, gibbsite and goethite. In depth samples (first and second feet), quartz, orthoclase feldspar, microcline feldspar, hematite, monazite and zircon were observed. The major minerals quartz and feldspars are presented invariably in all the samples of all depth samples. The minor minerals sepiolite and the iron bearing minerals *viz.* hematite, magnetite and goethite are identified. Hence, the XRD results are agreed with the FTIR analysis.

Horizontal and vertical (upper, first and second feet samples) distribution of magnetic susceptibility: The measured magnetic susceptibility values for all depth samples are shown in Fig. 7 and are ranged from 5.5×10^{-8} m^3/kg to 507×10^{-8} m^3/kg, 4.58×10^{-8} m^3/kg to 396.36×10^{-8} m^3/kg and 4.35×10^{-8} m^3/kg to 39.51×10^{-8} m^3/kg for the upper surface, first and second feet, respectively. Seven upper surface sites (S_6, S_7, S_{21}-S_{23}, S_{25} and S_{33}) and only two sites (S_6 and S_{22}) from first feet samples exhibit the high magnetic susceptibility values ($>100 \times 10^{-8}$ m^3/kg) [36], which may be purely related to anthropogenic activities such as traffic effluents, emissions from vehicles, industry and fossil fuel combustions [8]. High magnetic susceptibility values are observed in all foot of Mahabalipuram (S_{22}) (Fig. 7). Spatial distributions of magnetic susceptibility in first and second feet samples almost follow the same trend observed in the upper surface. As expected, magnetic susceptibility levels fall as one move from upper to second feet. Lu & Bai [37] measured the magnetic susceptibility in surface sediments of Hangzho city, China. They also revealed the similar findings,

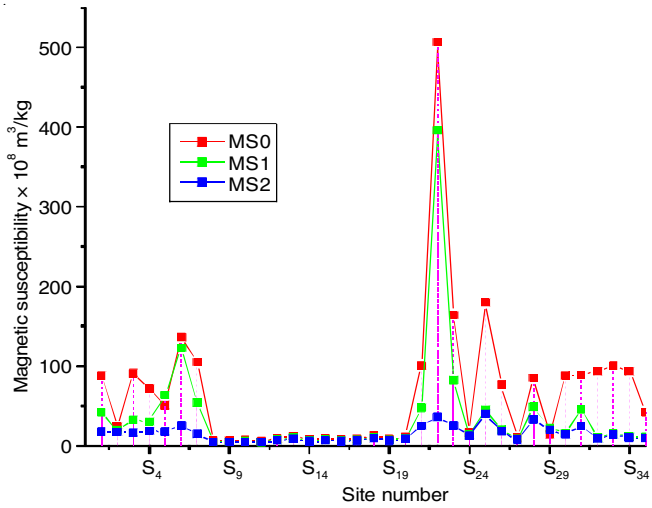

Fig. 7. Magnetic susceptibility values for all depth samples

namely that increasing levels in surface sediments are mainly related to anthropogenic activity.

Multivariate statistical analysis

Pearson's correlation analysis: Pearson's correlations analysis was carried out to understand the inter-relationship between the radiological, mineralogical and magnetic parameters using the SPSS 16.0 windows software and observed results are tabulated in Table-3. A strong correlation between ^{238}U and ^{232}Th was observed in all depth samples, which may be due to the presence of monazite mineral in the study area [38]. A same strong correlation was obtained by Radhakrishna *et al.* [39], Baranwal *et al.* [40], Uosif *et al.* [16] and Ramasamy *et al.* [34] for Ullal, Chhatrapur, red sea and Kerala beach sediments, respectively. In first and second feet, a positive and poor correlation exists between ^{232}Th & ^{40}K and ^{238}U & ^{40}K, indicate that ^{40}K concentrations may not be related with the presence of ^{232}Th & ^{238}U bearing mineral. The same poor correlation between these radionuclides was also observed by Mohanty *et al.* [38] and Ramasamy *et al.* [34]. Existence of high positive correlation between absorbed dose rate and ^{238}U and ^{232}Th concentration in all depth samples shows that total radioactivity level is mainly controlled by these two radionuclides rather than ^{40}K. The same trend was observed by Ramasamy *et al.* [14] in Kerala beach sediments. Quartz and Microcline feldspar are poorly correlated, whereas Kaolinite is moderately correlated with ^{40}K (Table-4). Paramasivam *et al.* [13] successfully shown the dependence of radionuclide concentrations on the magnetic susceptibility in sediment. In present beach, magnetic suscepti-

TABLE-3
PEARSON'S CORRELATION ANALYSIS AMONG RADIOACTIVITY VARIABLES, EXTINCTION COEFFICIENT OF MAJOR MINERALS AND MAGNETIC SUSCEPTIBILITY IN DIFFERENT DEPTH BEACH SEDIMENTS

Upper surface								
	U0	Th0	K0	D0	EQ0	EMF0	EK0	MS0
U0	1							
Th0	0.978	1						
K0	-0.142	-0.064	1					
D0	0.971	0.997	0.015	1				
EQ0	-0.465	-0.467	-0.126	-0.477	1			
EMF0	-0.194	-0.102	0.618	-0.057	0.118	1		
EK0	0.162	0.157	0.651	0.214	-0.229	0.359	1	
MS0	0.720	0.723	0.125	0.736	-0.384	0.019	0.032	1
First feet								
	U1	Th1	K1	D1	EQ1	EMF1	EK1	MS1
U1	1							
Th1	0.781	1						
K1	0.220	0.370	1					
D1	0.786	0.998	0.422	1				
EQ1	-0.173	-0.142	-0.033	-0.142	1			
EMF1	-0.157	-0.143	0.274	-0.123	0.203	1		
EK1	0.243	0.078	0.411	0.107	0.075	0.343	1	
MS1	0.606	0.881	0.312	0.876	-0.300	-0.293	-0.052	1
Second feet								
	U2	Th2	K2	D2	EQ2	EMF2	EK2	MS2
U2	1							
Th2	0.590	1						
K2	0.311	0.266	1					
D2	0.657	0.967	0.496	1				
EQ2	-0.070	-0.012	-0.218	-0.069	1			
EMF2	0.019	0.235	0.320	0.281	0.273	1		
EK2	-0.049	0.052	0.488	0.159	-0.195	0.327	1	
MS2	0.656	0.632	0.521	0.719	-0.387	0.086	0.122	1

Note: U0, U1, U2, Th0, Th1, Th2, K0, K1, K2 respectively represents the concentrations of ^{238}U, ^{232}Th and ^{40}K (Bq/kg) in upper, first and second feet samples; D0, D1 and D2 respectively represents absorbed dose rate (nGy/h) in upper, first and second feet samples; EQ0, EQ1, EQ2, EMF0, EMF1, EMF2, EK0, EK1 and EK2 respectively represents relative distribution of Quartz, Microcline Feldspar and Kaolinite in upper, first and second feet samples; MS0, MS1 and MS2 respectively represents magnetic susceptibility (m^3/kg) in upper, first and second feet samples.

TABLE-4
FACTOR ANALYSIS AMONG RADIOACTIVITY VARIABLES, EXTINCTION COEFFICIENT OF MAJOR MINERALS AND MAGNETIC SUSCEPTIBILITY IN DIFFERENT DEPTH BEACH SEDIMENTS

Variables	Components				
	1	2	3	4	5
U0	0.798	-0.370	-0.209	0.225	0.134
U1	0.711	-0.010	0.116	0.250	-0.166
U2	0.715	0.023	0.539	-0.049	-0.054
Th0	0.820	-0.303	-0.186	0.200	0.210
Th1	0.890	-0.086	0.195	0.273	0.004
Th2	0.405	0.268	0.566	-0.496	-0.228
K0	0.273	0.838	-0.062	0.001	0.010
K1	0.547	0.505	-0.067	-0.102	0.010
K2	0.582	0.518	-0.076	-0.009	-0.169
D0	0.845	-0.237	-0.193	0.205	0.205
D1	0.902	-0.050	0.184	0.260	0.000
D2	0.543	0.358	0.507	-0.431	-0.241
EQ0	-0.558	0.160	0.545	0.526	-0.038
EQ1	-0.358	0.362	0.421	0.591	-0.294
EQ2	-0.510	0.176	0.629	0.460	-0.042
EMF0	0.009	0.755	0.008	0.067	0.541
EMF1	-0.123	0.784	0.143	-0.044	0.547
EMF2	-0.081	0.764	0.222	-0.098	0.399
EK0	0.294	0.635	-0.469	0.153	-0.322
EK1	0.223	0.711	-0.480	0.183	-0.203
EK2	0.223	0.737	-0.466	0.179	-0.279
MS0	0.892	-0.123	0.200	0.038	0.170
MS1	0.885	-0.316	0.090	0.201	0.147
MS2	0.797	0.111	0.216	-0.317	-0.147
Eigen value	8.938	5.256	2.786	1.867	1.408
Variance (%)	37.240	21.902	11.607	7.781	5.867
Cumulative (%)	37.240	59.142	70.749	78.530	84.396

Note: U0, U1, U2, Th0, Th1, Th2, K0, K1, K2 respectively represents the concentrations of ^{238}U, ^{232}Th and ^{40}K (Bq/kg) in upper, first and second feet samples; D0, D1 and D2 respectively represents absorbed dose rate (nGy/h) in upper, first and second feet samples; EQ0, EQ1, EQ2, EMF0, EMF1, EMF2, EK0, EK1 and EK2 respectively represents relative distribution of Quartz, Microcline Feldspar and Kaolinite in upper, first and second feet samples; MS0, MS1 and MS2 respectively represents magnetic susceptibility (m^3/kg) in upper, first and second feet samples.

bility plays a vital role to fix the total radioactivity level since it is well correlated with ^{238}U and ^{232}Th concentrations and absorbed dose rate in all depth samples.

Factor analysis (FA): Factor analysis (FA) is also carried out to identify a smaller number of underlying dimensions, or factors that can be used to represent relationships among a set of interrelated variables. This analysis is actually performed on the correlation matrix between different parameters (same parameters which are used in Pearson's Correlations analysis are taken) followed by varimax normalized rotation using the SPSS 16.0 windows software. Table-4 presents the factor loadings, as well as their relevant explained variance which shows that five components with eigen value > 1, explaining 84.396 % of the total variance. The first two components show high eigen values such as 8.938 (37.24 % of total variance) and 5.256 (21.902 % of total variance). Concentrations of ^{238}U and ^{232}Th, calculated absorbed dose and measured magnetic susceptibility in all studied depths are accumulated in component 1 with high positive loadings. The ^{40}K concentration and amount of quartz of all feet were also accumulated in component 1 with moderate positive and negative loading, respectively. It is confirm that concentrations of ^{238}U and ^{232}Th and magnetic susceptibility could be the controlling factors for total radioactivity. The parameters like ^{40}K concentration, amount of microcline feldspar and kaolinite in all feet are presented with positive loading in component 2. It shows that these parameters are least contributors for the total radioactivity. Components 3, 4 and 5 are not taken for discussions because of its lower eigen values.

From the statistical analyses, it is confirmed that magnetic susceptibility plays a major role in controlling the radioactivity values of present beach sediments. According to Paramasivam *et al.* [13] and Suresh *et al.* [41], magnetic minerals could be enriched in lower grain sized (120 μm) samples. Moreover, several studies [20,41-45] were confirmed that the activity concentration of radionuclides decreased as the grain size of sediments decreased in different beach, coast and river sediments. Therefore, present study has intended to measure the level of radioactivity after removal of < 125 μm fractions from selected samples of upper surface.

Radioactivity levels of > 125 μm grain sized samples separated from upper surface: For this analysis, the upper surface samples were subjected into grain size separation analysis (1000 to 63 μm) by standard procedure and weight percentage of individual grain size is calculated for all the site samples (Table-5). The activity concentrations of same ^{238}U, ^{232}Th and ^{40}K (Table-6) in > 125 μm grain sized sediments of 15 randomly selected sampling sites from upper surface were measured by γ-ray spectroscopic analysis. It is observed that the activity concentrations are significantly lowered when compared with the respective values of the bulk samples (before the removal of < 125 μm grain sized particles *i.e.* upper surface) (Fig. 8) as reported in the literature.

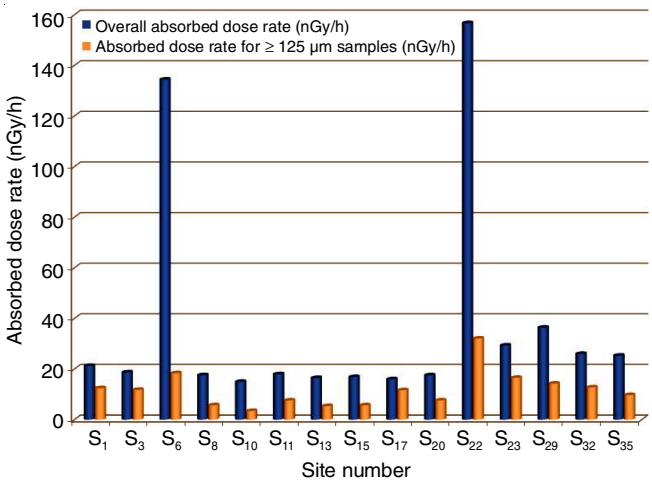

Fig. 8. Comparison of calculated absorbed dose rate for bulk and ≥ 125 μm removed samples from selected sites from upper surface

Conclusion

The radiological, mineralogical and magnetic susceptibility measurement analyses have been successfully carried out spatially and vertically using the standard techniques. The γ-ray spectroscopic analysis shows that average of all the radiological

TABLE-5
WEIGHT PERCENTAGE OF VARIOUS GRAIN SIZED SAMPLES AND wt.% OF MAGNETIC MINERALS OF ALL SITES OF UPPER SURFACE SAMPLES

Site number	Weight percentage of various grain sizes								Total (%)	Wt.% of ≥ 125 μm
	1000 μm	710 μm	500 μm	300 μm	210 μm	125 μm	90 μm	63 μm		
S_1	1.2	4.3	20.6	47.8	19.7	4.4	1.2	0.5	99.7	6.1
S_2	1.7	8.6	13.8	49.4	20.1	5.0	0.7	0.3	99.6	6.0
S_3	1.3	7.2	9.0	61.4	13.4	5.8	1.2	0.5	99.8	7.5
S_4	1.0	2.2	10.0	52.4	26.3	6.0	1.0	0.7	99.6	7.7
S_5	1.5	0.8	12.5	43.1	30.2	9.3	1.5	0.8	99.7	11.6
S_6	1.0	1.4	12.8	37.0	28.2	14.9	2.6	1.8	99.7	19.3
S_7	3.0	12.0	16.4	43.0	19.7	4.0	1.0	0.6	99.7	5.6
S_8	8.6	18.5	26.5	27.5	14.2	3.0	1.0	0.6	99.7	4.6
S_9	3.0	3.5	15.5	42.4	30.3	4.2	0.8	0.2	99.9	5.2
S_{10}	3.7	6.3	15.7	44.0	24.6	3.6	1.2	0.8	99.9	5.6
S_{11}	2.8	14.6	42.1	32.5	5.3	1.2	0.6	0.5	99.6	2.3
S_{12}	2.0	10.3	46.4	30.7	7.2	1.5	1.0	0.5	99.6	3.0
S_{13}	1.1	6.8	21.5	56.5	11.5	1.2	0.8	0.5	99.9	2.5
S_{14}	1.6	8.7	30.4	44.0	12.4	1.3	1.0	0.3	99.7	2.6
S_{15}	1.3	9.5	36.1	39.6	10.2	1.5	1.0	0.5	99.7	3.0
S_{16}	1.2	4.8	30.5	37.0	21.6	2.4	1.5	0.5	99.5	4.4
S_{17}	2.1	6.6	43.8	30.0	13.0	2.6	0.7	0.8	99.6	4.1
S_{18}	1.2	5.8	39.7	29.0	19.4	2.6	1.4	0.5	99.6	4.5
S_{19}	1.5	4.6	34.0	34.6	21.7	2.0	1.2	0.3	99.9	3.5
S_{20}	1.0	2.4	9.4	46.7	36.2	2.7	1.0	0.4	99.9	4.3
S_{21}	1.0	7.9	18.3	31.7	31.4	7.3	1.3	1.0	99.9	9.6
S_{22}	1.2	10.3	12.6	17.2	34.6	21.2	1.2	1.5	99.8	23.9
S_{23}	0.5	0.8	4.2	51.1	37.7	5.2	1.0	0.5	99.9	6.7
S_{24}	1.3	8.2	20.6	37.6	27.4	3.0	1.3	0.4	99.8	4.7
S_{25}	1.0	7.6	26.4	36.2	22.7	3.0	1.8	1.2	99.9	6.0
S_{26}	1.6	10.3	27.8	35.3	19.3	3.9	1.2	0.5	99.9	5.6
S_{27}	1.3	8.6	29.6	34.2	20.4	4.2	1.0	0.5	99.8	5.7
S_{28}	1.4	7.2	33.1	35.6	17.2	3.2	1.0	1.0	99.7	5.2
S_{29}	1.7	4.2	13.2	36.0	34.8	4.3	3.1	2.5	99.8	9.9
S_{30}	1.2	3.7	16.9	32.2	36.4	4.2	2.8	1.5	98.9	8.5
S_{31}	1.0	4.6	18.3	39.2	30.7	3.3	2.0	0.5	99.6	5.8
S_{32}	0.7	5.7	19.3	36.0	34.1	2.5	1.0	0.5	99.8	4.0
S_{33}	1.0	5.2	22.7	51.4	14.3	4.0	1.0	0.2	99.8	5.2
S_{34}	0.8	4.7	26.5	44.5	18.3	3.6	1.0	0.4	99.8	5.0
S_{35}	1.0	8.0	21.7	35.5	27.6	5.2	0.6	0.2	99.8	6.0

TABLE-6
ACTIVITY CONCENTRATIONS OF ^{238}U, ^{232}Th AND ^{40}K WITH THEIR UNCERTAINTIES FOR ≥ 125 μM RANDOMLY SELECTED SAMPLES FROM UPPER SURFACE

Site number	Activity concentration (Bq/kg)		
	^{238}U	^{232}Th	^{40}K
S_1	5.73 ± 4.76	6.33 ± 4.39	143.74 ± 25.63
S_3	5.68 ± 4.42	6.58 ± 4.43	124.48 ± 14.12
S_6	8.47 ± 4.62	11.87 ± 4.94	174.36 ± 18.86
S_8	BDL	BDL	136.78 ± 14.71
S_{10}	BDL	BDL	82.22 ± 14.16
S_{11}	BDL	5.76 ± 4.68	98.32 ± 16.21
S_{13}	BDL	BDL	128.46 ± 24.38
S_{15}	BDL	BDL	136.33 ± 24.50
S_{17}	5.84 ± 4.46	6.72 ± 4.48	116.51 ± 24.64
S_{20}	BDL	BDL	182.60 ± 24.68
S_{22}	10.76 ± 4.81	28.34 ± 4.38	239.44 ± 24.72
S_{23}	6.49 ± 4.51	6.65 ± 4.26	228.67 ± 24.70
S_{29}	BDL	5.98 ± 4.48	254.92 ± 24.84
S_{32}	BDL	5.76 ± 4.62	222.62 ± 25.64
S_{35}	BDL	BDL	233.49 ± 25.14

parameters (concentrations of ^{238}U, ^{232}Th and ^{40}K and calculated absorbed dose rate) were within the recommended level in all studied feet. However, some extreme values were observed in upper surface and first feet of S_6 and S_{22} due to the presence of black sands. Various activity concentration trends are observed from surface to second feet depth. However, mean activity concentration of ^{238}U was decreased, while ^{40}K was increased towards the deep with random variation of ^{232}Th. The FTIR and XRD analyses exhibit the presence of eleven minerals in all feet sediments. The amount of quartz and feldspar is decreased and kaolinite is increased from upper to deeper depth (first and second feet) due to weathering and leaching of quartz and feldspar. Due to anthropogenic activities, upper surface samples have higher magnetic susceptibility value when compared with depth samples. Statistical analysis confirmed that magnetic susceptibility plays a major role in controlling the radioactivity values of present beach sediments. The activity concentration of ^{238}U, ^{232}Th and ^{40}K of > 125 μm grain sized

sediments from upper surface are significantly lowered when compared with the respective values of the bulk samples.

ACKNOWLEDGEMENTS

The authors are thankful to The Director, IGCAR and Head, HASD, Indira Gandhi Centre for Atomic Research, Kalpakkam, for granting the permission to use the γ-ray spectrometer; HOD, Department of Physics, Annamalai University for grant permission to use the FTIR spectroscopic technique and The Director, Centre of Advanced Study in Marine Biology, Faculty of Marine Sciences, Annamalai University, Annamalai Nagar, India for granting the permission to use MS2B meter for magnetic susceptibility measurements.

CONFLICT OF INTEREST

The authors declare that there is no conflict of interests regarding the publication of this article.

REFERENCES

1. H.K. Shuaibu, M.U. Khandaker, T. Alrefae and D.A. Bradley, *Mar. Pollut. Bull.*, **119**, 423 (2017); https://doi.org/10.1016/j.marpolbul.2017.03.026
2. M. Al Shaaibi, J. Ali, N. Duraman, B. Tsikouras and Z. Masri, *Mar. Pollut. Bull.*, **168**, 112442 (2021); https://doi.org/10.1016/j.marpolbul.2021.112442
3. M. Radomirovic, S. Stankovic, M. Mandic, M. Jovic, L.J. Mandic, S. Dragovic and A. Onjia, *Mar. Pollut. Bull.*, **169**, 112491 (2021); https://doi.org/10.1016/j.marpolbul.2021.112491
4. UNSCEAR, United Nations Scientific Committee on the Effect of Atomic Radiation, Sources and Effects of Ionizing Radiation, Report to General Assembly, with Scientific Annexes, United Nations, New York (2000).
5. J. Wang, J. Du and Q. Bi, *Mar. Pollut. Bull.*, **114**, 602 (2017); https://doi.org/10.1016/j.marpolbul.2016.09.040
6. M.L. Martínez, A. Intralawan, G. Vázquez, O. Pérez-Maqueo, P. Sutton and R. Landgrave, *Ecol. Econ.*, **63**, 254 (2007); https://doi.org/10.1016/j.ecolecon.2006.10.022
7. C. Small and R.J. Nicholls, *J. Coast. Res.*, **19**, 584 (2003).
8. V. Ramasamy, S. Senthil, K. Paramasivam and G. Suresh, *Acta Ecol. Sin.*, **42**, 57 (2022); https://doi.org/10.1016/j.chnaes.2021.03.006
9. V. Ramasamy, S. Senthil, V. Meenakshisundaram and V. Gajendran, *Res. J. Appl. Sci. Eng. Technol.*, **1**, 54 (2009).
10. V. Ramasamy, S. Senthil and V. Meenakshisundaram, *Arab J. Basic Appl. Sci.*, **1**, 15 (2009).
11. V. Ramasamy, S. Senthil, G. Suresh and V. Meenakshisundaram, *Carpath. J. Earth Environ. Sci.*, **7**, 137 (2012).
12. A. Papadopoulos, A. Koroneos, G. Christofides, L. Papadopoulou, I. Tzifas and S. Stoulos, *J. Environ. Radioact.*, **162-163**, 235 (2016); https://doi.org/10.1016/j.jenvrad.2016.05.035
13. K. Paramasivam, V. Ramasamy and G. Suresh, *Appl. Radiat. Isot.*, **149**, 130 (2019); https://doi.org/10.1016/j.apradiso.2019.04.025
14. N. Krishnamoorthy, S. Mullainathan, M.A.E. Chaparro, M.A.E. Chaparro and R. Mehra, *Environ. Earth Sci.*, **76**, 286 (2017); https://doi.org/10.1007/s12665-017-6606-9
15. C. Booth, J. Walden, A. Neal and J. Smith, *Sci. Total Environ.*, **347**, 241 (2005); https://doi.org/10.1016/j.scitotenv.2004.12.042
16. M.A.M. Uosif, A. El-Taher and A.G.E. Abbady, *Radiat. Prot. Dosimetry*, **131**, 331 (2008); https://doi.org/10.1093/rpd/ncn175
17. R.A. Sutherland and E. de Jong, *Health Phys.*, **58**, 417 (1990); https://doi.org/10.1097/00004032-199004000-00004
18. G.T. Cook, M.S. Baxter, H.J. Duncan and R. Malcolmson, *J. Environ. Radioact.*, **1**, 119 (1984); https://doi.org/10.1016/0265-931X(84)90003-1
19. Y. Örgün, N. Altinsoy, S.Y. Sahin, Y. Güngör, A.H. Gültekin, G. Karahan and Z. Karacik, *Appl. Radiat. Isot.*, **65**, 739 (2007); https://doi.org/10.1016/j.apradiso.2006.06.011
20. C. Tsabaris, G. Eleftheriou, V. Kapsimalis, C. Anagnostou, R. Vlastou, C. Durmishi, M. Kedhi and C.A. Kalfas, *Appl. Radiat. Isot.*, **65**, 445 (2007); https://doi.org/10.1016/j.apradiso.2006.11.006
21. M. Jankovic, D. Todorovic and M. Savanovic, *Radiat. Meas.*, **43**, 1448 (2008); https://doi.org/10.1016/j.radmeas.2008.03.004
22. V. Ramasamy, M. Sundarrajan, K. Paramasivam, V. Meenakshisundaram and G. Suresh, *Appl. Radiat. Isot.*, **73**, 21 (2013); https://doi.org/10.1016/j.apradiso.2012.11.014
23. S.P. Gupta, Statistical Methods, Sultan Chand & Sons, Educational Publishers, New Delhi (2001).
24. V. Ramasamy, K. Paramasivam, G. Suresh and M.T. Jose, *Spectrochim. Acta A Mol. Biomol. Spectrosc.*, **117**, 340 (2014); https://doi.org/10.1016/j.saa.2013.08.022
25. W.D. Keller and E.E. Pickett, *Am. Mineral.*, **34**, 855 (1949).
26. H.H. Adler and P.F. Kerr, *Am. Mineral.*, **47**, 700 (1962).
27. J.D. Russell, V.C. Farmer and B. Velde, *Mineral. Mag.*, **37**, 869 (1970); https://doi.org/10.1180/minmag.1970.037.292.01
28. J. Hlavay, K. Jonas, S. Elet and J. Inczedy, *Clays Clay Miner.*, **26**, 139 (1978); https://doi.org/10.1346/CCMN.1978.0260209
29. S.A. Fysh and P.M. Fredericks, *Clays Clay Miner.*, **31**, 377 (1983); https://doi.org/10.1346/CCMN.1983.0310507
30. J.D. Russell, eds.: M.J. Wilson, Infrared Methods-A Hand Book of Determinative Methods in Clay Mineralogy, Blackie & Sons Ltd., New York, p. 133 (1987).
31. D. Beaufort, A. Cassagnabere, S. Petit, B. Lanson, J.C. Lacharpagne G. Berger and H. Johansen, *Clay Miner.*, **33**, 297 (1998); https://doi.org/10.1180/000985598545499
32. J. Madejova, *Vib. Spectrosc.*, **31**, 1 (2003); https://doi.org/10.1016/S0924-2031(02)00065-6
33. V. Ramasamy, P. Rajkumar and V. Ponnusamy, *Indian J. Phys.*, **83**, 1295 (2009); https://doi.org/10.1007/s12648-009-0110-3
34. V. Ramasamy, M. Sundarrajan, G. Suresh, K. Paramasivam and V. Meenakshisundaram, *Appl. Radiat. Isot.*, **85**, 1 (2014); https://doi.org/10.1016/j.apradiso.2013.11.119
35. V. Ramasamy, M. Sundarrajan, K. Paramasivam and G. Suresh, *Appl. Radiat. Isot.*, **95**, 159 (2015); https://doi.org/10.1016/j.apradiso.2014.10.023
36. T. Yang, Q. Liu, L. Chan and Z. Liu, *Environ. Geol.*, **52**, 1639 (2007); https://doi.org/10.1007/s00254-006-0609-2
37. S.G. Lu and S.Q. Bai, *J. Appl. Geophys.*, **60**, 1 (2006); https://doi.org/10.1016/j.jappgeo.2005.11.002
38. A.K. Mohanty, D. Sengupta, S.K. Das, S.K. Saha and K.V. Van, *J. Environ. Radioact.*, **75**, 15 (2004); https://doi.org/10.1016/j.jenvrad.2003.09.004
39. A.P. Radhakrishna, H.M. Somashekarappa, Y. Narayana and K.A. Siddappa, *Health Phys.*, **65**, 390 (1993); https://doi.org/10.1097/00004032-199310000-00006
40. V.V. Baranwal, S.P. Sharma, D. Sengupta, M.K. Sandilya, B.K. Bhaumik, R. Guin and S.K. Saha, *Radiat. Meas.*, **41**, 602 (2006); https://doi.org/10.1016/j.radmeas.2006.03.002
41. G. Suresh, V. Ramasamy and V. Meenakshisundaram, *Appl. Radiat. Isot.*, **70**, 556 (2012); https://doi.org/10.1016/j.apradiso.2011.11.048
42. P. Blanco Rodriguez, F. Vera Tome, J.C. Lozano and M.A. Perez-Fernandez, *J. Environ. Radioact.*, **99**, 1247 (2008); https://doi.org/10.1016/j.jenvrad.2008.03.004
43. E.R. Van der Graaf, R.L. Koomans, J. Limburg and K. de Vries, *Appl. Radiat. Isot.*, **65**, 619 (2007); https://doi.org/10.1016/j.apradiso.2006.11.004
44. P.K. Shetty, Y. Narayana and K. Siddappa, *J. Environ. Radioact.*, **86**, 132 (2006); https://doi.org/10.1016/j.jenvrad.2005.08.002
45. R.A. Ligero, I. Ramos-Lerate, M. Barrera and M. Casas-Ruiz, *J. Environ. Radioact.*, **57**, 7 (2001); https://doi.org/10.1016/S0265-931X(00)00213-7